Astron. Astrophys. 244, 501–510 (1991)

ASTRONOMY AND ASTROPHYSICS

Photospheric dynamics and the NLTE formation of the solar K I 769.9 nm line

M.T. Gomez[1], R.J. Rutten[2] and G. Severino[1]

[1] Osservatorio Astronomico di Capodimonte, Via Moiariello 16, I-80131 Napoli, Italy
[2] Sterrekundig Instituut, Postbus 80000, NL-3508 TA Utrecht, The Netherlands

Received July 6, accepted September 15, 1990

Abstract. We extend earlier analyses of the K I 769.9 nm resonance line as a diagnostic of dynamical phenomena in the solar photosphere by evaluating the effects of dynamical variations on departures from LTE in the K I spectrum. We employ representative models for the solar granulation and the solar five-minute oscillation to estimate dynamical NLTE departures in the K I populations and to compare these to standard plane-parallel NLTE modeling. Various NLTE mechanisms operate together in K I simultaneously with fortuitous cancellations; the resulting population departures vary less than 30% between dynamical perturbations. Our results validate the assumption of departure invariance, i.e. adopting NLTE population departure coefficients from a standard static model for use in dynamical perturbations, as a good first-order approximation in K I 769.9 nm formation studies.

Key words: radiation transfer – helioseismology – Sun (the): atmosphere of – convection – line formation

1. Introduction

The K I resonance line at 769.9 nm represents one of the few photospheric resonance lines present in the optical solar spectrum. Its core is formed in the upper photosphere near the temperature minimum and its flanks are sensitive both to the granulation and to the five-minute *p*-mode oscillations, making the line into an important diagnostic of convective phenomena (e.g. Roca-Cortes et al. 1983; Andersen et al. 1985; LoPresto & Pierce 1985; Bonet et al. 1988; Bonet et al. 1989) and for helioseismology (e.g. Brookes et al. 1978; Jefferies et al. 1988; Pallé et al. 1989; Isaak et al. 1989).

Such diagnostic usage requires study of the response of the 769.9 nm line to the dynamical processes in the solar photosphere. Pertinent dynamical line formation studies including solar granulation and solar oscillations have been performed at Naples, viz. Marmolino et al. (1984), Severino et al. (1986), Marmolino et al. (1987), Gomez et al. (1987), and Marmolino et al. (1988). In these papers a standard plane-parallel static model of the solar photosphere was perturbed with velocity, temperature and pressure fluctuations obtained from dynamical wave and granule models. Spectral line profiles were then synthesized from these perturbed models and compared with observations.

A complication in such studies is the presence of departures from local thermodynamic equilibrium (LTE) in the line formation; for K I 769.9 nm the importance of NLTE processes has been known since the pioneering study by de la Reza & Müller (1975). NLTE effects were taken into account in the series of Naples papers listed above, but with the simplifying assumption that the NLTE departures are not changed by the dynamical perturbations, i.e. that the NLTE population departure coefficients b_i remain the same between the static and perturbed models for every level i and at every height. With that assumption the atomic level populations are simply obtained by multiplying the perturbed LTE populations with the departure coefficients found for the standard model, without solving the NLTE radiative transfer in detail within the dynamical perturbations. This assumption of departure invariance is the topic of this paper.

The same assumption has also been made in analyses of solar Fe I lines (Canfield 1976; Keil & Canfield 1978; Cram et al. 1979; Keil & Marmolino 1986; Marmolino & Stebbins 1989). The major NLTE process affecting Fe I lines is ultraviolet overionization (Lites 1972, cf. Rutten 1988) which reduces line opacities compared to LTE while the line source functions remain close to the Planck function. Departure invariance was thought valid for Fe I because such overionization is non-local in nature: the ionizing radiation fields should sense a large enough volume to wash out perturbations of small horizontal extent. However, the detailed Fe I line synthesis by Nordlund (1984) based on numerical simulations of the granulation has shown that the difference between the effective NLTE iron ionization temperature and the electron temperature varies substantially with horizontal temperature fluctuations, even on subgranular scales: cool surface elements produce much larger radiative overionization in the layers above them than hot elements do. This result for Fe I leads us to question in this paper whether similar modulation effects affect the formation of K I 769.9 nm.

The NLTE formation of the K I resonance line in static models is the reverse of the Fe I pattern: the line extinction coefficient is close to the Saha-Boltzmann LTE value throughout the photosphere but the line source function drops well below the Planck function. This drop is due to photon losses and displays typical resonance-line scattering behaviour. The drop sets in far below the $\tau = 1$ level and the line source function in higher layers is more strongly controlled by the temperature at this deep

Send offprint requests to: G. Severino

"thermalization level" than by the temperature at the $\tau = 1$ formation level. Assuming that the line source function and the emergent radiation scale with the local Planck function is therefore questionable when the perturbations affect the temperature at these two levels differently, or when perturbations induce large departure changes; an example of the latter is given in Fig. 3a of Scharmer (1984). Furthermore, K I has at 4.34 eV the smallest ionization energy of all abundant elements. It is predominantly ionised throughout the photosphere, and any perturbations which change NLTE ionization processes affect the K I population departures as well.

Thus, detailed modeling is required to test the assumption of NLTE departure invariance also for K I. We do that here, and we so make another step along the (long) way from plane-parallel static LTE modeling to pluridimensional dynamic NLTE modeling. We make our study differential in character by computing full NLTE statistical equilibrium solutions first for a static reference model and then for perturbation models of the granulation and the five-minute oscillation, following the earlier papers of the Naples group. The perturbations specify the fluctuations in temperature and pressure associated with the inhomogeneity; together with its height-dependent velocity, a *dynamic* model of line formation results (cf. Cram 1981) rather than a *kinematic* one in which only the velocity effects are accounted for. We display and interpret the population differences between the static and the perturbed models, both for changes in temperature, pressure and velocity separately and for the combined perturbations.

Our results are indicative of what occurs in reality, although we cannot make a direct comparison with observations because the latter suffer from spatial and temporal averaging not taken into account here. We also neglect the horizontal averaging of radiation fields which may take place within the solar atmosphere itself by not permitting lateral photon exchange between adjacent structures: we describe line formation here by using the perturbed models as if they are plane-parallel. This "1.5-dimensional" multicomponent approach may lead to overestimation of NLTE effects, especially those in higher layers which depend on contrasts in radiation generated much deeper down if such contrasts are washed out along the way up. Although detailed pluridimensional analyses (e.g. Mihalas et al. 1978; Owocki & Auer 1980; Jones & Skumanich 1980) validated such multicomponent modeling for exponential atmospheres, other results (Kneer 1981; Jones 1986) indicate that this issue is yet unresolved. However, our analysis is schematic in any case since we employ simplified models of solar inhomogeneities; our goal here is to study the validity of the assumption of departure invariance, and not to reproduce the true inhomogeneous photosphere in overly sophisticated detail.

The next section specifies our input. Section 3 shows results, for the K I populations and also for the 769.9 nm resonance line. We discuss our findings in Sect. 4.

2. Input models

2.1. Static modeling

We use a simplified atomic model for K I consisting of only five levels plus continuum; it is shown in the inset of Fig. 1. It is similar to the atomic model specified by Severino et al. (1986) with the following improvements: (i) all bound-free radiative rates are now computed in detail (data from Wiese et al. 1969), while the $5s^2\,S^e$, $3d^2\,D^e$ and $5p^2\,P^o$ photoionization rates were evaluated from fixed radiation fields before; (ii) the $5s^2\,S^e$—$5p^2\,P^o$ and $3d^2\,D^e$—$5p^2\,P^o$ bound-bound radiative transitions are now included, also from Wiese et al. (1969); (iii) depth-dependent Van der Waals broadening is taken into account in computing the extinction profile, multiplying the classical value by three as advised by Holweger & Müller (1974).

We describe the K I NLTE line formation processes in the solar photosphere in more detail in a forthcoming paper (Bruls et al. in preparation); both larger and smaller atomic models are analysed there as well as the various mechanisms which populate and depopulate the K I levels. That work shows that the simplified model atom used here suffices to study NLTE phenomena differentially; it retains the basic ingredients necessary to produce a sufficiently accurate description of NLTE processes in the lower K I levels.

We solve the coupled statistical equilibrium equations and radiative transfer equations assuming complete redistribution, the temperature, gas pressure, and electron number density for the static case from the VAL3C model atmosphere of Vernazza et al. (1981), without turbulent pressure and without microturbulent line broadening, and we adopt the potassium abundance value given by Allen (1976): $N_K = 8.91\ 10^{-8}\,N_H$.

A difference with Severino et al. (1986) is that we now use the NLTE radiative transfer code MULTI implemented by Carlsson (1986). It is based on Scharmer's approximate operator perturbation technique (Scharmer 1981; Scharmer 1984; Scharmer & Carlsson 1985) and it permits the presence of velocity gradients. We have tested the code against the Naples version of LINEAR Auer et al. (1972) and obtain the same results for benchmark VAL3C computations – but with a substantial increase in speed, the new code giving an impressive order of magnitude saving in CPU usage. Figure 1 shows VAL3C results which we discuss in Sect. 3.

2.2. Perturbations

The perturbations which we apply to the VAL3C model as schematic representations of the solar granulation and the solar five-minute oscillation are shown in Figs. 2a and 2b, respectively. The *granulation* model displays the familiar property of granulation that its temperature contrast vanishes quickly with height while the vertical velocity difference persists much higher up. The model is symmetric: granules and intergranules are defined to have equal areas but opposite velocities and opposite temperature and pressure perturbations. The depth-dependent granular temperature perturbation ΔT and the velocity v differ from those of Gomez et al. (1987): $\Delta T/T$ now reaches 20% at $h = -50$ km instead of 7% at $h = 0$ km, while v increases inward to 2.5 km s^{-1} at $h = -100$ km rather than leveling off at 2 km s^{-1} below $h =$ 0 km. These changes represent more vigorous granulation in the deep layers, in accordance with the numerical models of Nelson (1978) and Steffen et al. (1989). The pressure fluctuations $\Delta P/P$ are computed from the kinetic energy density $\Delta P \sim \rho v_z^2$ because, in the anelastic approximation for thermal convection, in a subsonic circulation the pressure fluctuations must do sufficient work to convert vertical into horizontal motion by destroying the vertical kinetic energy (Gough 1969). The corresponding density fluctuations are shown in Fig. 2a. A hot rising granule is less dense than the unperturbed atmosphere only in the deepest

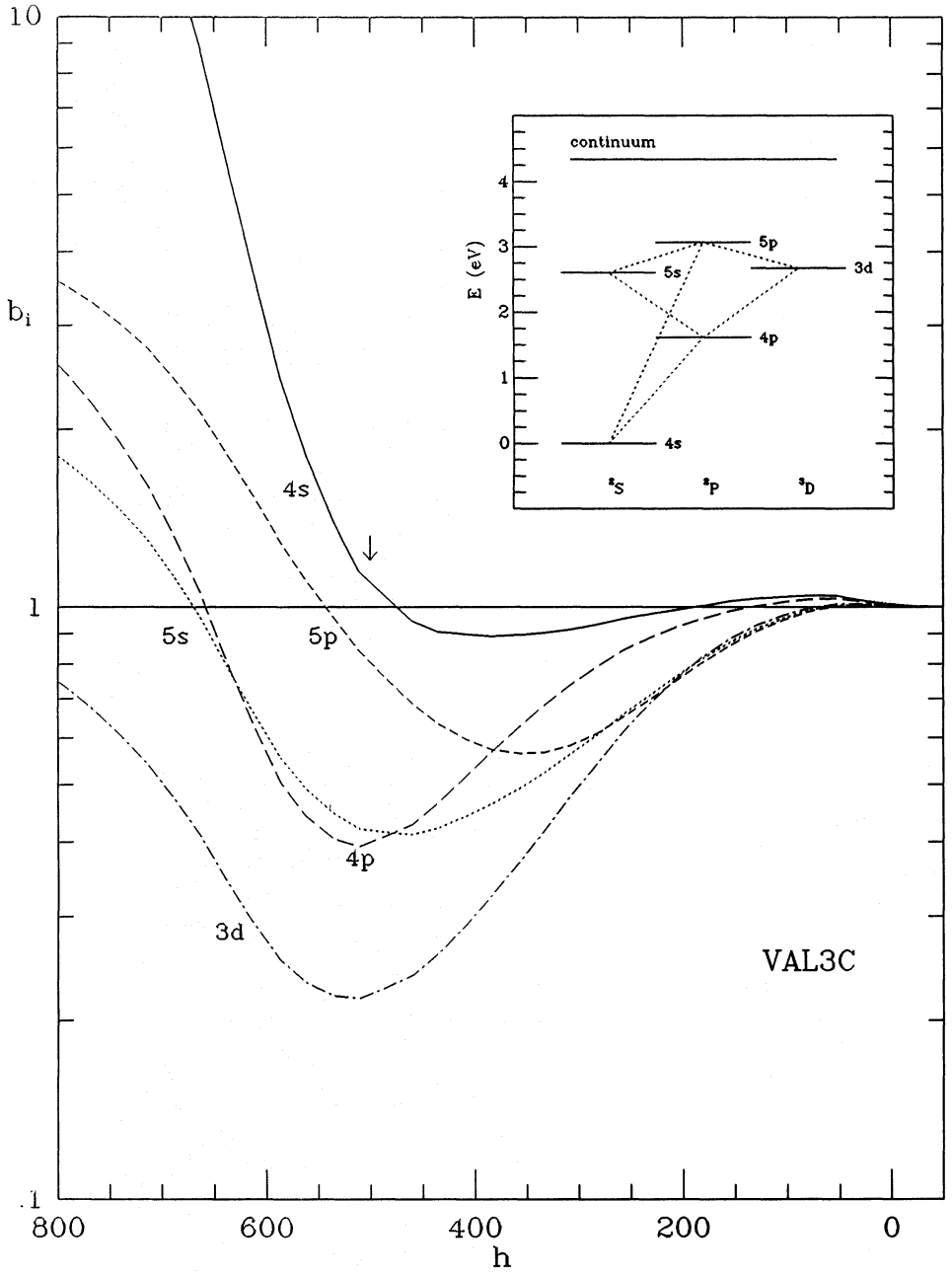

Fig. 1. K I NLTE departure coefficients for the VAL3C atmospheric model against height. The arrow for $4s^2S^e$ specifies the height where the 769.9 nm resonance line reaches line-center optical depth unity. The inset shows the K I model atom used in this paper

layers of the photosphere where $\Delta T/T > \Delta P/P$, but it is denser higher up; a cool sinking intergranule has opposite behavior.

To represent the *five-minute oscillation* we adopt the equations describing an adiabatic monochromatic linear wave in a stratified isothermal medium following Eqs. 3–9 of Gomez et al. (1987). In contrast to that paper we neglect radiative damping here, but account for the temperature variation through the photosphere by entering the local temperature of the VAL3C model into the sound velocity, and thus into the scale height, cutoff frequency, Brunt-Väisälä frequency and the polarization relations. Notice that the vertical velocity amplitude at $h = 0$ km ($\tau_{5000} = 1$) is chosen equal to 0.35 km s^{-1} (cf. Canfield 1976). Our model is admittedly simple: this way of entering temperature variations smoothes the wave amplitudes and does not account for wave reflections; also, the adiabaticity implies neglect of radiative damping so that the temperature fluctuations are overestimated in the deep photosphere. Nevertheless, the model contains the basic elements of the solar *p*-mode oscillations and is therefore a suitable representation for our differential study. Since the temperature and pressure fluctuations of an adiabatic evanescent wave are plus and minus ninety degrees out of phase with the velocity, respectively (e.g. Stein & Leibacher 1980), we present results for the two extreme phases of the oscillation: (i) the *rarefaction phase* corresponding to minimum pressure, maximum temperature, and zero velocity, and (ii) the *compression phase* corresponding to maximum pressure, minimum temperature, and zero velocity. The phase shift between the temperature and pressure fluctuations implies that their effects on the density add up, as shown in Fig. 2 where the $\Delta\rho/\rho$ curve holds for the compression phase.

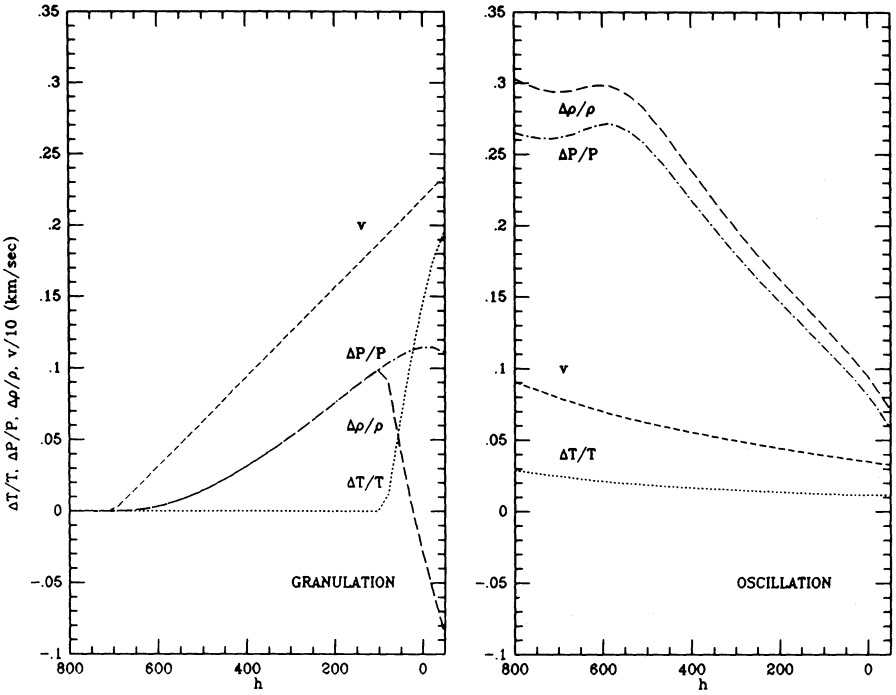

Fig. 2. Amplitudes of the temperature, pressure, density, and velocity fluctuations against height, respectively for the granulation perturbation (left) and the oscillation perturbation (right). The perturbation for an intergranular region is the same as the granulation perturbation, but with opposite signs. Symmetry is also adopted for the oscillation perturbations; the temperature and pressure are ninety degrees out of phase with the velocity. The density fluctuation shown here (long dash) corresponds to the compression phase of the wave, i.e. maximum ΔP, minimum (negative) ΔT and zero velocity

We obtain perturbed model atmospheres by adding the ΔT and ΔP fluctuations to the temperature and pressure stratification of the VAL3C atmosphere. The electron pressure is recomputed from the new temperature and gas pressure by evaluating the ionization balance of 15 elements, adopting standard abundances taken from Withbroe (1971). These balances are first computed assuming LTE and are then approximately corrected for NLTE effects (which are appreciable in the temperature minimum region of the VAL3C model due to radiative overionization of the electron donors) by multiplication with the ratio P_e/P_e^{LTE} computed from the VAL3C model itself. A test in which we enter the differences between the VAL3F and VAL3C models as a perturbation of the latter shows that this procedure reproduces the electron pressure of the VAL3F model to within 30%. We also neglect NLTE departures in the hydrogen background opacity because their effect on the K I populations is only of order 1%. We then compute the perturbed density following Eqs. 89–90 of Vernazza et al. (1973) and obtain a new mass column density scale by integration. Finally, the velocity perturbation is entered directly into the MULTI input.

3. Results

3.1. Reference model

Figure 1 shows results for the VAL3C model in the form of NLTE departure coefficients b_i per level i plotted against height. The departure coefficients are defined as usual by $b_i \equiv (n_i/n_i^{\mathrm{LTE}})/(n_c/n_c^{\mathrm{LTE}})$, with n_i the actual population of level i and n_i^{LTE} the population of level i computed from the Boltzmann & Saha equations. The similar ratio for the K II ground level population n_c enters as normalization factor; these "Menzel" b-values are scaled to the next higher ion and not to the total element abundance which is sometimes misleading (cf. Vernazza et al. 1981, p. 663), but not for K I because K II is the majority species throughout the photosphere: the Menzel b-coefficients and the β-coefficients of Wijbenga & Zwaan (1972) are virtually identical for K I. In this case the line extinction coefficient scales with the lower level departure coefficient b_l as $\kappa \approx b_l \kappa^{\mathrm{LTE}}$. The line source function scales with the ratio of the upper and lower level departure coefficients: $S \approx (b_u/b_l)\, B_\nu$. Both relations are exact when stimulated emission is negligible.

The NLTE departure behaviour in Fig. 1 agrees with previous NLTE modeling of the K I atom (de la Reza & Müller 1975; Shchukina 1981; Shchukina & Aleksandrova 1982; McKenna 1984; Severino et al. 1986; Shchukina 1987; Shchukina et al. 1990). A comprehensive discussion of K I radiative transfer in the solar photosphere will be given by Bruls et al. (in preparation); here, we briefly summarize pertinent conclusions from that analysis.

There are various NLTE mechanisms that operate together to reach statistical equilibrium and so determine the K I populations. A major driving mechanism is given by the photon losses in the $4s^2\,S^e - 4p^2\,P^o$ resonance lines which tend to overpopulate the ground level at the expense of the $4p^2\,P^o$ upper levels. These population losses are partially replenished out of the reservoir available in the K II ground level in which most solar potassium resides. This replenishment uses photo-recombination to the $3d^2\,D^e$ level and radiative cascade to $4p^2\,P^o$ as primary channel. Such photon-loss driven recombination is termed "photon suction" by Bruls et al. It is the reverse of photon (or "optical") pumping in which incoming line photons overexcite higher levels from a lower reservoir; in photon suction, outgoing line photons draw extra atoms down into lower levels from a higher reservoir. In potassium it feeds the $4p^2\,P^o$ and $4s^2\,S^e$ levels from the K II ground level, and it so changes the partitioning between K I and K II. The process is neutralized by extra photoionization, mainly from the $4p^2\,P^o$ level. Its bound-free edge at 455 nm is characterized by an appreciable $J_\nu - B_\nu$ excess, large enough to provide

sufficient net ionization to obtain statistical equilibrium while $4p^2\,P^o$ is underpopulated.

These NLTE mechanisms operate together to produce the equilibrium population patterns seen in Fig. 1. The departure coefficients start at unity in the deep photosphere where all radiation fields are thermal. Various coefficients drop outward due to line photon losses; in particular, the $4p^2\,P^o$ coefficient drops away from $4s^2\,S^e$ already below $h=200$ km, much deeper than the 769.9 nm $\tau=1$ level (arrow), due to strong resonance scattering. The departure coefficient of $3d^2\,D^e$ falls deepest of all; this level provides the main replenishment channel to $4p^2\,P^o$. Above $h=500$ km all coefficients rise steeply because LTE ionization overestimates true ionization by a large amount in the chromosphere.

Special behaviour is shown by the $5p^2\,P^o$ level of which the departure curve shows an early outward rise due to strong optical pumping in the $4s^2\,S^e-5p^2\,P^o$ line at 404.5 nm by radiation with a large $J_\nu-B_\nu$ excess. (It was overestimated by Severino et al. 1986 due to their neglect of the $5s^2\,S^e-5p^2\,P^o$ and $3d^2\,D-5p^2\,P^o$ transitions.)

These K I population departure patterns differ from the typical NLTE patterns that neutral metals such as Fe I display in the photosphere. The reasons for this distinction are first that the photoionization cross-section from the $4s^2\,S^e$ ground level of K I is abnormally small due to deviations from central-field potentials through cancellations (e.g. Seaton 1951), and second that the K I resonance lines become optically thin already in the upper photosphere and effectively thin already in the deep photosphere, so that their photon losses act as driver throughout the whole photosphere. Similar behaviour occurs in solar Na I (Gehren 1975; Caccin et al. 1980).

A striking result seen also in Fig. 1 is that the population of the $4s^2\,S^e$ ground level remains close to its LTE value throughout the photosphere. This LTE behaviour does not mean that the K I ground level obeys LTE strictly but it is the fortuitous net result of the uneasy balance between resonance-line photon suction and violet pumping. In fact, Fig. 1 shows slight $4s^2\,S^e$ underpopulation while the computations of Bruls et al. with a more comprehensive model atom produce a small overpopulation; the net result is rather sensitive to the details of the computation.

The overall trends of the K I departure coefficients with height shown in Fig. 1 are not altered substantially by our perturbations. We therefore display the relative changes $\Delta b/b=(b_{\rm perturbed}/b_{\rm VAL3C})-1$ in the following sections; negative values of $\Delta b/b$ in Figs. 3 and 4 imply downward shifts of the corresponding curves in Fig. 1.

3.2. *Granulation*

Figure 3 shows results from our granulation perturbations, the positive perturbation (hot rising granule) at left and the negative perturbation (cool sinking integranule) at right. The top panels show the relative changes in departure coefficients, first for each parameter alone, i.e. temperature, pressure and velocity fluctuation, and then for the combined change with all three perturbations applied together. Note that electron number and gas densities are recomputed also for the single parameter changes. The bottom panels show the changes in the resulting line source functions for the 769.9 nm resonance line.

The granular temperature change has the largest effect. It dominates the total change, it is largest for the $4s^2\,S^e$ and $4p^2\,P^o$ resonance-line levels, and its effects are larger for the intergranule (top right) than for the granule (top left), with an initial sign reversal for the intergranule. Let us first discuss these temperature effects. The granular temperature perturbation stops already at $h=100$ km, as shown in Fig. 2a; at that height, the upper and lower departure coefficients of the resonance lines divert only slightly from each other ($4s^2\,S^e$ and $4p^2\,P^o$ in Fig. 1) which shows that the NLTE driving by resonance-line photon suction is just starting there. Thus, the *whole* height range in which NLTE effects are important lies above our granular temperature perturbation; it is only through the coupling to continuum radiation formed in the deepest layers that the K I NLTE departures sense the presence of granulation. That coupling is primarily through the net photoionization from $4p^2\,P^o$ and the pumping of $5p^2\,P^o$ which are sensitive to the continuum near 400 nm. This continuum arises from the very deep photosphere (see Ayres 1989 for an interesting discussion of this point) and becomes optically thin already within the granular temperature perturbation, as evident from the abrupt change in temperature effects at $h=100$ km: above this level, the fractional departure corrections change less because the pertinent radiation fields have already been set. The hot radiation emerging from the granule provides a larger violet $J_\nu-B_\nu$ excess than for VAL3C, so that statistical equilibrium is reached already for a smaller $4p^2\,P^o$ population. The balance between photon suction replenishment and violet overionization at which statistical equilibrium is reached shifts towards overionization; smaller K I populations result.

The larger $J_\nu-B_\nu$ excess also affects the pumping of $5p^2\,P^o$, as evident from the bulge in its curve (upper left in Fig. 3). It peaks at the temperature minimum where the extra radiation feeds enough extra atoms upward to compensate for the overall K I population decrease. This pumping also affects the other levels appreciably. A test computation without the pump (cutting out the $4s^2\,S^e-5p^2\,P^o$ transition, results not shown) produces $4s^2\,S^e$ population very close to LTE up to $h=400$ km for the VAL3C standard model, but separation of the $\Delta b/b$ curves for the resonance line levels: the $4s^2\,S^e$ curve then lies above the $4p^2\,P^o$ curve throughout the upper photosphere. The overall spread of the various curves is much smaller without the pump; the latter adds excitation differences to the pattern set by the change in ionisation.

The same pattern is seen in reversal for the intergranule at right. In this case the balance shifts towards suction because the violet radiation is less superthermal in the upper photosphere; the smaller violet intensities above the intergranular temperature perturbation provide less ionisation so that balancing requires population increases compared to the reference atmosphere. The lack of violet radiation also decreases the $4s^2\,S^e-5p^2\,P^o$ pump, again producing near-equality of the $4s^2\,S^e$ and $4p^2\,P^o$ curves throughout the photosphere. Without the pump (results not shown) there is again appreciable difference: the curves for the lower levels separate while the overall spread becomes much smaller.

The intergranule curves show a small sign reversal in the deepest layers which is caused by a reversal of the $J_\nu-B_\nu$ excess for the $4p^2\,P^o$ bound-free transition due to the steep temperature perturbation of our model: the intergranular temperature-to-height relation has a local minimum at $h=0$ km. In addition, the lower temperature produces less ionization of electron donor elements and smaller H^-_{bf} opacity; the resulting inward shift of

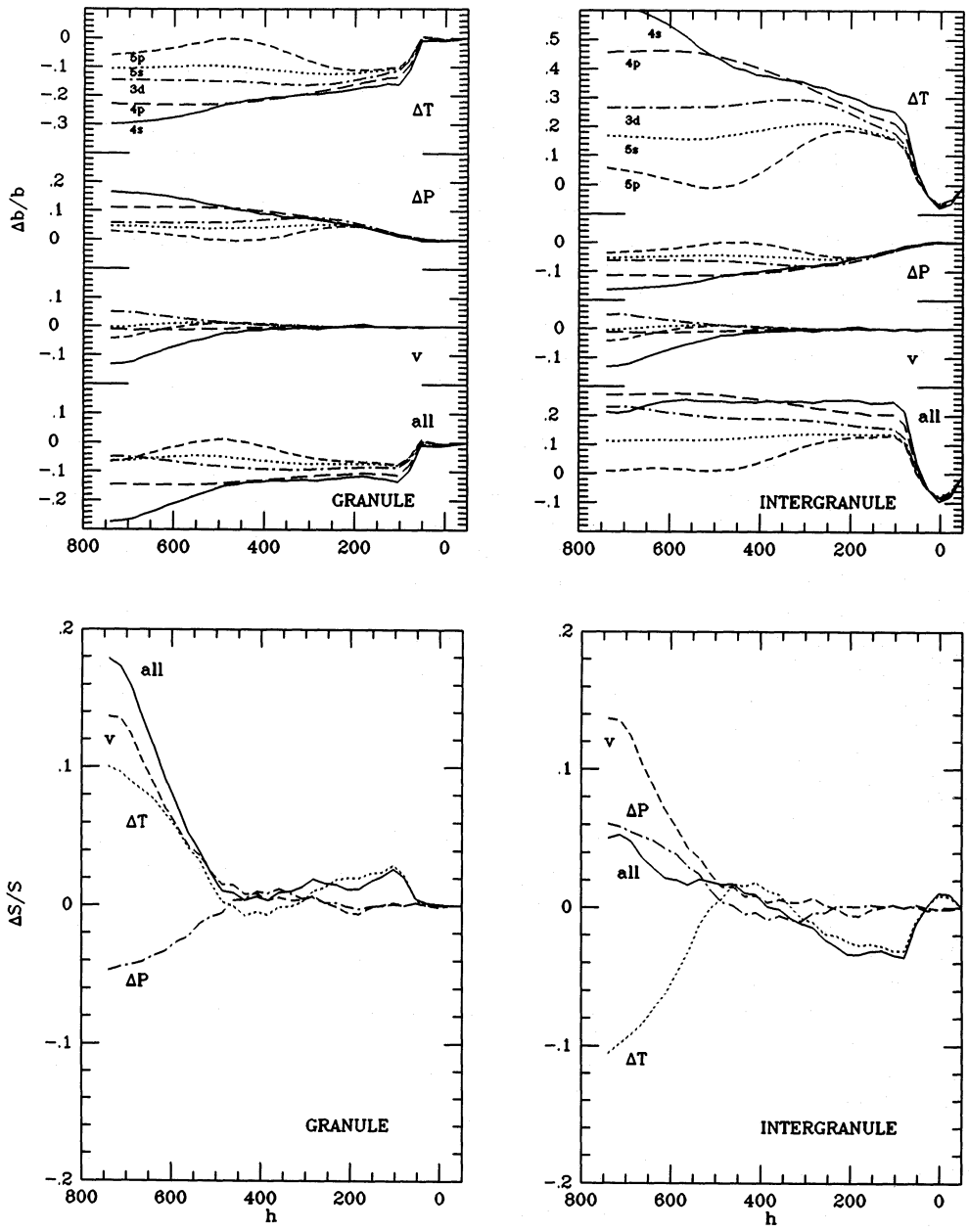

Fig. 3. Results for the granulation perturbations, respectively for a hot rising granule (left) and a cool sinking intergranule (right). The top panels show fractional departure changes $\Delta b/b = (b_{\text{perturbed}}/b_{\text{VAL3C}}) - 1$, first for the temperature, pressure and velocity perturbations separately and then for the combined perturbation. Curve coding specifies the different K I levels of the term diagram in Fig. 1. The bottom panels show the resulting change in NLTE behaviour of the 769.9 nm line source function. Curve coding as in Fig. 2; the solid lines are for the combined perturbations

the continuum formation height shifts the K I thermalisation depths to deeper layers so that the sign reversal is indeed followed by the departures. The deeper formation also increases the departure changes in the higher layers: the violet continua above the intergranule originate deeper down, respond to larger $\Delta T/T$ modulation, and produce larger fractional changes than for the granular perturbation at left.

The departure changes for the pure pressure perturbations (second row in Fig. 3) are similar in character to the pure temperature effects, but smaller in size and opposite in sign. They respond to changes in thermalization which follow from the increased density above a granule and also affect the $J_\nu - B_\nu$ behaviour; the overall balance shifts to larger suction effectivity and larger K I populations result. The curve of $5p^2P^o$ has a dip because the pump is less effective than for the VAL3C. The departure changes for the less dense intergranule at right show the reversed pattern.

The velocity effects (third row in Fig. 3) are yet smaller. They occur because shifted spectral lines see different radiation fields from below; the effects are symmetrical and the two sets of curves are identical.

The combined effects are shown in the fourth row of Fig. 3. The contributions from the temperature and pressure changes partially cancel each other and the resulting departure changes remain below 30% or 0.1 dex; thus, the overall departure pattern of Fig. 1 is only slightly affected. These changes affect the line extinction coefficients directly, but their effects on the line source functions are yet smaller. In particular, the upper and lower levels of the resonance lines ($4p^2P^o$ and $4s^2S^e$) have nearly equal departure changes throughout the photosphere; this fortuitous

equality results from the effect of the $4s^2S^e - 5p^2P^o$ pump on the $4s^2S^e$ departures. It implies that the 769.9 nm line source function is not affected at all. This is indeed shown in the lower panels of Fig. 3 which show the change in the 769.9 nm line source function, defined as

$$\frac{\Delta S}{S} = \frac{S/B - S_{\mathrm{VAL3C}}/B_{\mathrm{VAL3C}}}{S_{\mathrm{VAL3C}}/B_{\mathrm{VAL3C}}},$$

where we cancel the LTE variations by normalizing the perturbed and static line source functions S and S_{VAL3C} by the corresponding Planck functions. The remaining NLTE variations in the 769.9 nm source function (solid curves) are indeed quite small, or order 2% throughout the photosphere for the granule and less than 4% for the intergranule. Without the $4s^2S^e - 5p^2P^o$ pump (not shown) there are larger changes, reaching a decrease of 5% for the granular ΔS and a 7% increase for the intergranular ΔS in the upper photosphere.

3.3. *Oscillation*

Results for the oscillation perturbation are shown in Fig. 4. In the rarefaction phase (minimum pressure, maximum temperature and zero velocity) the slight temperature increase causes small population increases compared to the reference model (top left in Fig. 4). These departure changes are not set in the deep photosphere as was the case for the granule because the oscillation perturbation (Fig. 2 right) is just the reverse in character: its temperature enhancement increases outward. Its effect is also just the reverse. The violet radiation field from the deep photosphere

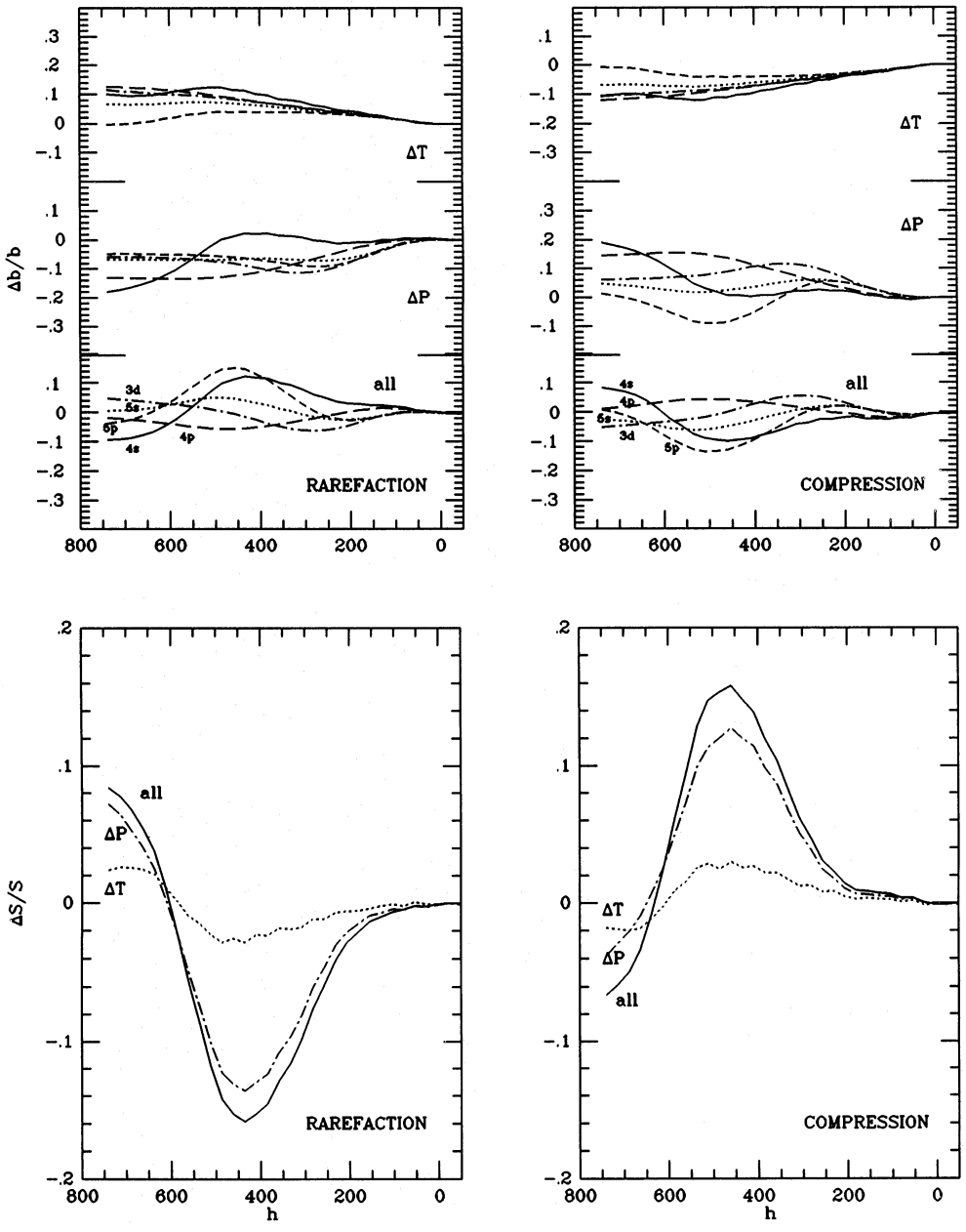

Fig. 4. Results for the oscillation perturbations, respectively for the rarefaction phase (left) and the compression phase (right). The top panels show fractional departure changes $\Delta b/b = (b_{\mathrm{perturbed}}/b_{\mathrm{VAL3C}}) - 1$, first for the temperature and pressure perturbations separately and then for the combined perturbation. Curve coding specifies the different K I levels of the term diagram in Fig. 1. The bottom panels show the resulting change in NLTE behaviour of the 769.9 nm line source function. Curve coding as in Fig. 2; the solid lines are for the combined perturbations

is not affected, but the larger temperature in the upper photosphere reduces the violet $J_\nu - B_\nu$ excess, the suction wins effectivity and larger populations are built up until the violet overionization reaches balancing from a sufficiently large $4p^2\,P^o$ population. There is again fine structure in the $4s^2\,S^e$ and $5p^2\,P^o$ curves due to the pump. The compression phase at right, with negative temperature perturbation, shows the same pattern in reverse.

The pressure effects are shown in the second row of Fig. 4. They are larger than the temperature effects and are set by the changes in thermalisation due to the large, outward increasing density changes. The rarefaction and compression effects are opposite and the resulting patterns differ in their height scaling because larger density implies higher thermalisation. An experiment without the $4s^2\,S^e - 5p^2\,P^o$ pump (results not shown) again produces appreciably smaller spread; the bulge in the $5p^2\,P^o$ granular curve then vanishes and the steep decline for $4s^2\,S^e$ in the chromosphere is reduced.

The temperature and pressure effects together (third row) enhance each other in the photosphere but the total changes remain small, less than 15%. There are no cancellation effects, however, and the fractional changes for the upper and lower levels of the resonance lines are not the same. This is evident from the 769.9 nm line source function changes shown in the bottom panels; the fractional change equals the population changes in amplitude and reaches about 15% in the temperature minimum. It is the same when the $4s^2\,S^e - 5p^2\,P^o$ pump does not operate.

3.4. *Line profiles*

In each panel of Fig. 5 we compare three sets of computed intensity profiles of the 769.9 nm line. The first set (solid curves) consists of the single profile from the reference VAL3C computation which produced the "static" NLTE departure coefficients shown in Fig. 1. It is shown in every panel to provide a reference for estimating the variations of the other profiles. This VAL3C profile is deeper than the observed disk-center solar profile, which reaches 17% of the continuum intensity, but we apply no spatial or temporal averaging here, nor microturbulent smearing of the local extinction coefficient or macroturbulent smearing of the emergent profile. With such parameters it is possible to obtain a good fit of the observed profile from the VAL3C model on the condition that the NLTE photon losses of this line are properly taken into account so that the computed profile is deep enough; computed LTE profiles are much too shallow (de la Reza & Müller 1975; Severino et al. 1986; Shchukina 1987). Our profiles are deeper yet and illustrate the perturbation effects at infinite resolution, which is fine for our differential NLTE study; they are not intended to serve as a gauge for upper-photospheric modeling (cf. Shchukina et al. 1990).

The second set (dot-dashed) are profiles computed from the perturbed models but using the static departure coefficients of Fig. 2, representing the assumption of departure invariance. The third set are the "full" NLTE profiles for which the radiative transfer and statistical equilibrium equations were solved explicitly. These correspond to the $\Delta b/b$ curves and $\Delta S/S$ curves labeled "all" in Figs. 3 and 4. The three sets are shown for the granule and the intergranule in the top panels and for the rarefaction and compression phases of the oscillation in the bottom panels, respectively.

Let us first discuss the differences between the static and the dynamic profiles. The main change for the wings of the profiles is given by the change in continuum intensity, which is appreciable both for the granulation and the oscillation perturbations. For the granulation this large modulation is primarily due to the large temperature perturbation in deep layers; for the oscillation the modulation reflects primarily the change in formation height produced by the density perturbation. The line flanks are primarily affected by the Doppler shifts. These are appreciable for the granulation since the granulation velocities persist to larger height than the temperature contrast. The resulting line center shifts are $-0.72\ \mathrm{km\,s^{-1}}$ for the granule and $+0.65\ \mathrm{km\,s^{-1}}$ for the intergranule. They are absent in the oscillation panels because the velocity is zero at all heights in the rarefaction and compression phases of our evanescent wave; in the intermediate phases (maximum velocity, zero pressure, and temperature changes) the Dopplershift of the emergent profile reaches $\pm 0.58\ \mathrm{km\,s^{-1}}$, corresponding to $\pm 1.5\,10^{-3}$ nm wavelength shift.

The differences between the simplified NLTE perturbation model, assuming departure invariance and using the departure coefficients from VAL3C, and the full NLTE computations are shown by the differences between the dash-dotted and dotted profiles. They are small, in agreement with the results above. The core intensities reflect the line source function at the corresponding $\tau = 1$ location and their changes are in agreement with the $\Delta S/S$ deviations seen in Figs 3 and 4: the differences are small for the granule and intergranule perturbations and reach about 20% for the oscillation. The differences are smaller in the wings, except for the inner wings of the intergranular profiles.

4. Conclusion

For all the apparent simplicity of the K I term diagram, the formation of the solar K I lines represents a relatively complex NLTE situation because there is competition between different NLTE mechanisms. That makes it difficult to predict the nature and size of population changes without detailed NLTE modeling. We have presented such modeling here for two sources of atmospheric parameter changes, the solar granulation and the solar five-minute oscillation. These are the major dynamical inhomogeneities affecting the solar photosphere and at the same time they provide two NLTE test cases of very different signatures, the granulation perturbing primarily the deep photosphere and the oscillation the upper photosphere.

We find that the NLTE population changes which result from the granulation and oscillation perturbations compared with standard plane-parallel NLTE modeling are largely set by the changes in the temperature for the granulation and the changes in pressure for the oscillation. They are largest for the granulation-type perturbation even though that affects the temperature only in deep layers, because such deep temperature changes affect the emergent violet radiation fields and control the amount of photoionization higher up. In addition, the effects of the $4s^2\,S^e - 5p^2\,P^o$ pump are important.

We have specifically tested the assumption of departure invariance made in various earlier papers by evaluating and analysing the NLTE departure changes compared to standard modeling. These changes are shown in Figs. 3 and 4 and are rather small, below 30%. This implies that simply using the

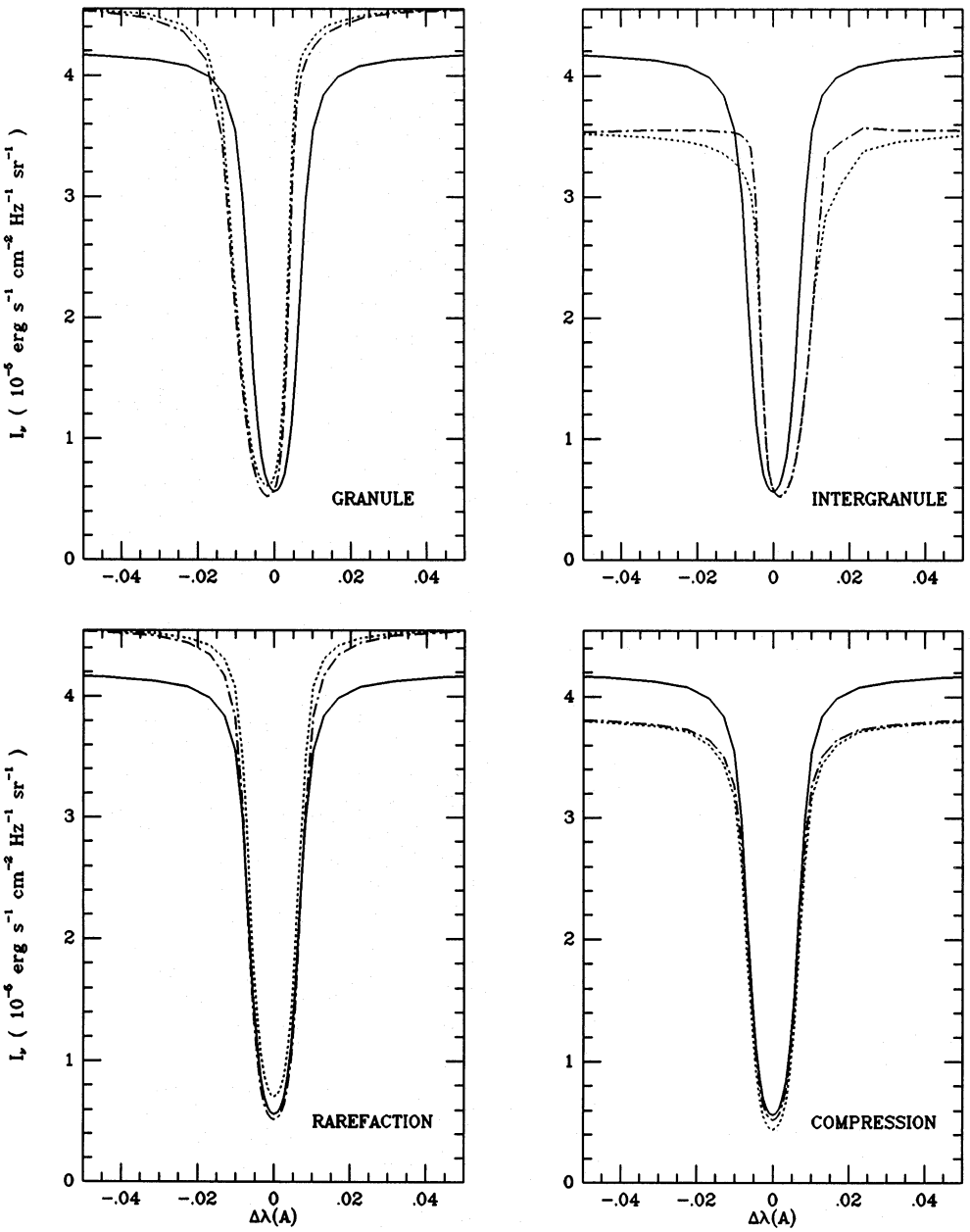

Fig. 5. Results for the K I 769.9 nm line, for the granulation perturbations (upper panels) and the oscillation perturbations (lower panels) respectively. The ordinate measures absolute intensity in erg s^{-1} cm^{-2} Hz^{-1} sr^{-1} *Solid*: reference VAL3C computation with the departure coefficients of Fig. 1, shown in each panel to facilitate comparison. *Dash-dotted*: perturbed atmosphere combined with the static departure coefficients of Fig. 1. *Dotted*: perturbed atmosphere with full NLTE solution

NLTE departure coefficients from plane-parallel modeling instead of computing detailed perturbation-dependent NLTE equilibria is in error by typically 20%. The errors are largest for the K I ground level and therefore affect the opacity of the 769.9 nm resonance line; the effect on the line source function is smaller for our granulation perturbation, due to fortuitous cancellation induced by the violet pumping of the $5p^2\,P^o$ level. With the pump, the core intensity of the 769.9 nm resonance line is rather insensitive to the granular temperature modulation.

In summary, the assumption of departure invariance is valid on the 20% accuracy level. In addition, this error estimate may be an overestimate because we have adopted "1.5-dimensional" radiative transfer here, neglecting lateral photon exchange. Thus, evaluating population departures from plane-parallel NLTE modeling represents a quite good first approximation to detailed pluridimensional NLTE modeling. The precise effects, however, are highly intricate.

Acknowledgements. We thank Drs. M. Carlsson and C. Marmolino for the use of their computer codes. R.J. Rutten is indebted to the Director of the Osservatorio Astronomico di Capodimonte for inviting him, and to its staff for their hospitality during his stay at Naples.

References

Allen C.W., 1976, Astrophysical Quantities, Athlone Press, University of London

Andersen B.N., Barth S., Hansteen V., Leifsen T., Lilje P.B., Vikanes F., 1985, Solar Phys. 99, 17

Auer L.H., Heasley J.N., Milkey R.W., 1972, A Computational Method for the Solution of Non-LTE Transfer Problems by the Complete Linearization Method, Contribution No. 555, Kitt Peak National Observatory
Ayres T.R., 1989, Solar Phys. 124, 15
Bonet J.A., Marquez I., Vazquez M., 1989, in: Solar and Stellar Granulation eds. R.J. Rutten, G. Severino, NATO ASI Series C-263, Kluwer, Dordrecht, p. 299
Bonet J.A., Marquez I., Vazquez M., Wöhl H., 1988, A&A 198, 322
Brookes J.R., Isaak G.R., van der Raay H.B., 1978, MNRAS 185, 1
Caccin B., Gomez M.T., Roberti G., 1980, A&A 92, 63
Canfield R.C., 1976, Solar Phys. 50, 239
Carlsson M., 1986, A Computer Program for Solving Multi-Level Non-LTE Radiative Transfer Problems in Moving or Static Atmospheres, Report No. 33, Uppsala Astronomical Observatory
Cram L.E., 1981, ApJ 247, 239
Cram L.E., Keil S.L., Ulmschneider P., 1979, ApJ 234, 768
de la Reza R., Müller E.A., 1975, Solar Phys. 43, 15
Gehren T., 1975, A&A 28, 289
Gomez M.T., Marmolino C., Roberti G., Severino G., 1987, A&A 188, 169
Gough D.O., 1969, J. Atmos. Sciences 26, 448
Holweger H., Müller E.A., 1974, Solar Phys. 39, 19
Isaak G.R., McLeod C.P., Pallé P.L., van der Raay H.B., Cortés T.R., 1989, A&A 208, 297
Jefferies S.M., Pallé P.L., van der Raay H.B., Regulo C., Cortés T.R., 1988, Nat 333, 646
Jones H.P., 1986, in: Small Scale Magnetic Flux Concentrations in the Solar Photosphere, eds. W. Deinzer, M. Knölker, H.H. Voigt, Abhandl. Akad. Wiss. Göttingen, Math.-Phys. Klasse Dritte Folge Nr. 38, Vandenhoeck und Ruprecht, Göttingen, p. 127
Jones H.P., Skumanich A., 1980, ApJS 42, 221
Keil S.L., Canfield R.C., 1978, A&A 70, 169
Keil S.L., Marmolino C., 1986, ApJ 310, 912
Kneer F., 1981, A&A 93, 387
Lites B.W., 1972, Observation and Analysis of the Solar Neutral Iron Spectrum, NCAR Cooperative Thesis No. 28, High Altitude Observatory, Boulder
LoPresto J.C., Pierce A.K., 1985, Solar Phys. 102, 21
Marmolino C., Roberti G., Severino G., 1987, Solar Phys. 108, 21
Marmolino C., Roberti G., Severino G., 1988, in: Physics of formation of FeII lines outside LTE, eds. R. Viotti, A. Vittone, M. Friedjung, Proc. IAU Coll. 94 (Capri), Reidel, Dordrecht, p. 217
Marmolino C., Roberti G., Vazquez M., Severino G., Wöhl H., 1984, in: Hydromagnetics of the Sun, ed. E. Rolfe, Proc. Fourth European Meeting on Solar Physics, Noordwijkerhout, The Netherlands, ESA-SP220, p. 191
Marmolino C., Stebbins R.T., 1989, Solar Phys. 124, 30
McKenna S.J., 1984, Ap&SS 106, 283
Mihalas D., Auer L.H., Mihalas B.R., 1978, ApJ 220, 1001
Nelson G.D., 1978, Solar Phys. 60, 5
Nordlund Å., 1984, in: Small-Scale Dynamical Processes in Quiet Stellar Atmospheres, ed. S.L. Keil, National Solar Observatory Summer Conference, Sacramento Peak Observatory, Sunspot, p. 181
Owocki S.P., Auer L.H., 1980, ApJ 241, 448
Pallé P.L., Hernández F.P., Cortés T.R., Isaak G.R., 1989, A&A 216, 253
Roca-Cortes T., Vazquez M., Wöhl H., 1983, Sol. Phys. 88, 1
Rutten R.J., 1988, in: Physics of Formation of FeII Lines Outside LTE, eds. R. Viotti, A. Vittone, M. Friedjung, IAU Colloquium 94, Reidel, Dordrecht, p. 185
Scharmer G.B., 1981, ApJ 249, 720
Scharmer G.B., 1984, in: Methods in radiative transfer, ed. W. Kalkofen, Cambridge University Press, Cambridge, p. 173
Scharmer G.B., Carlsson M., 1985, J. Comput. Phys. 59, 56
Seaton M.J., 1951, Proc. Royal Soc. London Series A 208, 418
Severino G., Roberti G., Marmolino C., Gomez M.T., 1986, Solar Phys. 104, 259
Shchukina N.G., 1981, Astrometriya & Astrofiz. 45, 13
Shchukina N.G., 1987, Kinematika Fiz. Nebesnykh Tel. 3, 40
Shchukina N.G., Aleksandrova I.I., 1982, Soln. Dannye Bull. 12, 100
Shchukina N.G., Shcherbina T.G., Rutten R.J., 1990, in: Solar Photosphere: Structure, Convection and Magnetic Fields, ed. J.-O. Stenflo, IAU Symposium 138 (Kiev), Kluwer, Dordrecht, p. 29
Steffen M., Ludwig H.-G., Krüß A., 1989, A&A 213, 371
Stein R.F., Leibacher J.W., 1980, in: Stellar Turbulence, eds. D.F. Gray, J.L. Linsky, IAU Coll. Nr. 51 (London), Lecture Notes in Physics 114, Springer, Berlin Heidelberg New York, p. 225
Vernazza J.E., Avrett E.H., Loeser R., 1973, ApJ 184, 605
Vernazza J.E., Avrett E.H., Loeser R., 1981, Ap&SS 45, 635
Wiese W.L., Smith M.W., Miles B.M., 1969, Atomic Transition Probabilities. Volume II, NSRDS-NBS 22, Natl. Bur. Standards, Washington
Wijbenga J.W., Zwaan C., 1973, Solar Phys. 23, 265
Withbroe G.L., 1971, in: The Menzel Symposium on Solar Physics, Atomic Spectra and Gaseous Nebulae, ed. K.B. Gebbie, Natl. Bur. Standards, Special Publ. 353, Washington, p. 127